

Ultrafast X-ray Diffraction of Transient Molecular Structures in Solution

H. Ihee,^{1*} M. Lorenc,² T. K. Kim,¹ Q. Y. Kong,² M. Cammarata,^{2,3}
J. H. Lee,¹ S. Bratos,⁴ M. Wulff²

We report direct structural evidence of the bridged radical ($\text{CH}_2\text{ICH}_2\cdot$) in a polar solution, obtained using time-resolved liquid-phase x-ray diffraction. This transient intermediate has long been hypothesized to explain stereochemical control in many association and/or dissociation reactions involving haloalkanes. Ultrashort optical pulses were used to dissociate an iodine atom from the haloethane molecule ($\text{C}_2\text{H}_4\text{I}_2$) dissolved in methanol, and the diffraction of picosecond x-ray pulses from a synchrotron supports the following structural dynamics, with ~ 0.01 angstrom spatial resolution and ~ 100 picosecond time resolution: The loss of one iodine atom from $\text{C}_2\text{H}_4\text{I}_2$ leads to the C-I-C triangular geometry of $\text{CH}_2\text{ICH}_2\cdot$. This transient $\text{C}_2\text{H}_4\text{I}$ then binds to an iodine atom to form a new species, the $\text{C}_2\text{H}_4\text{I-I}$ isomer, which eventually decays into $\text{C}_2\text{H}_4 + \text{I}_2$. Solvent dynamics were also extracted from the data, revealing a change in the solvent cage geometry, heating, and thermal expansion.

The prediction of molecular structures during a chemical reaction has progressed substantially because of advances in computational chemistry and molecular dynamics simulations (1). In contrast, direct structural characterization of short-lived reaction intermediates has only recently become accessible, with the advent of picosecond electron (2–5) and x-ray (6–11) diffraction techniques. These experiments are conducted using the pump and probe method: An ultrashort laser pulse initiates a reaction, and as it progresses, the diffraction signal from a delayed electron or x-ray pulse probes the change in the spatial correlations between atoms and molecules. Because the scattering cross section of electrons is high, electron diffraction is particularly useful for atoms and molecules in the gas phase (4, 5), thin films (3), and surfaces (2). However, the high cross section translates into shallow sample penetration, which makes it difficult for electrons to probe condensed samples such as liquids.

The scattering cross section of hard x-rays is six orders of magnitude lower than for electrons. Thus, x-rays can probe bulk samples, provided that the pulse intensity is sufficiently high, as is the case in our study using

synchrotron radiation (5×10^8 photons per pulse at 18 keV). The main difference between gas-phase and solution-phase diffraction is the relative concentration of excited molecules. In solution studies, scattering from the laser-excited solutes is typically well below 1% of the diffraction signal from the solvent. With a typical pump-pulse excitation efficiency of 10%, only about 1 in 1000 molecules is excited. The laser-induced signal is thus embedded in a strong background from non-excited molecules, which limits the signal-to-noise ratio of the diffraction data. In addition, structural rearrangements in the solvation shell complicate deconvolution of the solute and solvent signals.

Most reactions relevant to biology and industrial applications occur in the solution phase, and the chemistry of reactions in solution is extremely rich because of the complex solvent interactions with the solute. Although ultrafast optical spectroscopy (12, 13) has provided a wealth of information regarding the time scale for these processes, x-ray diffraction offers direct insight into the three-dimensional (3D) structures of transient intermediates, as well as solvent shell rearrangements.

We have applied time-resolved liquid-phase x-ray diffraction to the elimination reaction of 1,2-diiodoethane ($\text{C}_2\text{H}_4\text{I}_2$), which gives an iodine atom and a short-lived iodoethyl radical ($\text{CH}_2\text{ICH}_2\cdot$) intermediate in solution (14). Haloethyl radicals such as $\text{CH}_2\text{ICH}_2\cdot$ play a crucial role in the stereoselectivity of certain chemical processes (15–19). Skell and co-workers proposed a bridged structure for the radical, which is distinct from the classical anti structure, in order to explain the stereochemistry of free-radical addition reactions

(20). However, despite numerous theoretical (21–23) and experimental investigations (14, 24–26), direct structural evidence for the bridged structure has been lacking. Here, time-resolved x-ray diffraction data provide such evidence, together with the associated solvent dynamics.

To follow the structural dynamics during the course of the reaction, we collected time-resolved diffraction data for time delays of -3 ns, -100 ps, 100 ps, 300 ps, 1 ns, 3 ns, 10 ns, 30 ns, 50 ns, 70 ns, 100 ns, 300 ns, 1 μs , and 3 μs . The data point at -3 ns served as a (nonexcited) reference point, and another point at negative time delay (-100 ps) was collected to check the timing at high resolution. To recover the changes from the laser excitation only, difference signals were generated by subtracting the reference data at -3 ns from the data at any other time delay (27).

The image at -100 ps shows no difference intensity, as expected (Fig. 1). At positive times, difference features emerge and progress with time. After radial integration of the 2D difference images to 1D difference curves, $\Delta S(q)$, these curves were multiplied by q to magnify the intensity at high scattering angles [$q = (4\pi/\lambda)\sin(2\theta/2)$, where λ is the x-ray wavelength and 2θ the scattering angle]. The $q\Delta S(q)$ curves contain direct q -space information on the structural changes in the solute and in the solvent. It is more intuitively helpful to examine the sine-Fourier transforms, $r\Delta S(r)$, of the $q\Delta S(q)$ curves, where r is the interatomic distance. This representation corresponds to the change in the atom-atom pair distribution functions during the course of the reaction (28) and is a measure, biased by the x-ray form factor, of the change in the electron density around an (average) excited atom, as a function of r . There are three contributions to the measured signal (Fig. 2, A and B): the structural change in the solute, the change in the solvation cage caused by solute/solvent interaction, and the bulk solvent response to heating and thermal expansion.

To explain the experimental data theoretically and fit the measured signal, we included all known components to the signal. Specifically, we included not only the contributions from the solutes, but also the contribution to the signal from the heating of the surrounding solvent by calculating the temperature and density of the bulk solvent as a function of time (27). For the solute, we considered all possible reaction pathways. Upon photoexcitation, the parent solute molecule $\text{C}_2\text{H}_4\text{I}_2$ can dissociate through three possible channels: (i) a new transient species $\text{C}_2\text{H}_4\text{I}$ and an I atom, (ii) $\text{C}_2\text{H}_4 + 2\text{I}$, and (iii) $\text{C}_2\text{H}_4 + \text{I}_2$. Because $\text{C}_2\text{H}_4\text{I}$ is not stable, it can further dissociate into $\text{C}_2\text{H}_4 + \text{I}$, or it can bind to a free I atom to form a $\text{C}_2\text{H}_4\text{I-I}$ isomer. In summary, we can have the following solute species: $\text{C}_2\text{H}_4\text{I}_2$, $\text{C}_2\text{H}_4\text{I}$, C_2H_4 , $\text{C}_2\text{H}_4\text{I-I}$, I, and I_2 .

¹Department of Chemistry and School of Molecular Science (BK21), Korea Advanced Institute of Science and Technology (KAIST), Daejeon, 305-701, Republic of Korea. ²European Synchrotron Radiation Facility, Grenoble Cedex 38043, Boite Postal 220, France. ³National Institute for the Physics of Matter and Department of Physical and Astronomical Sciences, via Archirafi 36, 90123, Palermo, Italy. ⁴Laboratoire de Physique Théorique des Liquides, Université Pierre et Marie Curie, Case courrier 121, 4, Place Jussieu, Paris Cedex 75252, France.

*To whom correspondence should be addressed. E-mail: hyotcher.lihee@kaist.ac.kr

Theoretical scattering curves from these species, which include the change in solute and solvent cage structure, were obtained from molecular dynamics (MD) simulations (11), in which the system was set up to be in quasi-thermodynamic equilibrium at all times. Perturbation of the solvation cage can be expressed as a change in the atom-atom distance distribution between solute/solvent pairs. The changes in solute structure account for only part of the total signal, because of the presence of the solvent. In addition, the energy released from the photon-absorbing solute molecules causes a change in the temperature, pressure, and density of the solvent as a function of time. The shifts in intermolecular positions in the solvent are very small, on the milliangstrom length scale, but given the huge excess of solvent molecules over solutes, the integrated solvent signal can be comparable to or larger than the solute signal. A quantitative description of these solvent effects was also obtained from MD simulations (11).

Once all the components were obtained from MD simulations, the experimental data were fit to a sum of these components, with constraints to ensure conservation of total energy in the x-ray-probed volume (27). The hydrodynamics of the solvent, expressed through the time-dependent solvent temperature and density, were mathematically related to the solute dynamics through time-dependent solute concentrations, which lead to release of energy into the solvent during the solute reactions. Instead of fitting the data at each time point separately, data at all time delays were linked and fitted globally. Global fitting parameters included the rate coefficients. In Fig. 1, the fitting results for all time points are shown; more detailed depictions are given for the 100-ps time delay in Fig. 2, A and B. More detailed decompositions for other time points are given in (27). The fit yields, as a function of time, the change in concentration of putative solutes and the change in temperature and density of the bulk solvent (Fig. 2, E and F).

Figure 2, C and D, shows the major components in the fits. The first two curves from the top represent the change in the bulk solvent $\{q[\partial S(q)/\partial T]_V$ and $q[\partial S(q)/\partial \rho]_T\}$, where T is temperature, ρ is density, and V is volume. The other three curves represent the change related to the reaction channels: ($C_2H_4I_2 \rightarrow C_2H_4I + I$), ($C_2H_4I_2 \rightarrow C_2H_4I-I$), and ($C_2H_4I_2 \rightarrow C_2H_4 + I_2$). These curves bear imprints of the change in both solute and cage structure. According to the result of the least-square fit, C_2H_4I and I are the dominant solute species at 100 ps, and the formation of C_2H_4 or I_2 is not observed. This new transient C_2H_4I does not decay through the formation of $C_2H_4 + I$; rather, it reacts with an iodine atom to form a new species, the C_2H_4I-I isomer, with a

bimolecular rate constant of $2.1 (\pm 0.3) \times 10^{12} M^{-1}s^{-1}$, which is larger by two orders of magnitude than the rate constant for non-geminate formation of molecular iodine (29). The nascent isomer becomes the dominant solute species after a few nanoseconds. Eventually, this isomer also decays into $C_2H_4 + I_2$ in microseconds, with the rate constant of $4.8 (\pm 0.9) \times 10^5 s^{-1}$.

The characteristic (Gaussian-like) time constant of the solvent density change was 33 ± 5 ns and depends on the size of the laser beam and the speed of sound in the solvent (27); the fit gives 83 ± 10 μm (full width at half maximum) for the size of the laser beam, which is in agreement with the value measured by scanning the laser profile.

Initially (< 10 ns), the temperature and pressure of the solvent build up at fixed volume and density, a process expressed in the first component, $q[\partial S(q)/\partial T]_V$, in Fig. 2, C and D. The peaks and valleys in r space are mainly ascribed to a broadening of the atom-atom distributions $O \cdots O$ and $O \cdots C$ (where \cdots indicates an interatomic pair) at constant volume

between adjacent methanol molecules. Then the thermal expansion progresses with the observed time constant, and the solvent eventually returns to ambient pressure at a slightly expanded volume (and therefore decreased density) after about 100 ns {the second curve, $q[\partial S(q)/\partial \rho]_T$, in Fig. 2, C and D}. The peaks and valleys are caused by shifts in the interatomic distributions of $O \cdots O$ and $O \cdots C$ in the solvent.

After the thermal expansion, the solvent density has decreased by 2.1 kg m^{-3} (0.26%), which corresponds to a temperature rise of 1.8 K. Because we have determined the concentration of the end product $C_2H_4 + I_2$ to be 3.3 mM, and given that each decay $C_2H_4I_2^* \rightarrow C_2H_4 + I_2$ (where * indicates an excited state) releases 4.30 eV of energy, these transitions account for a temperature rise of 0.68 K in the solvent rather than the observed 1.8 K. We assign this difference to an invisible component in this experiment at 100-ps resolution: fast geminate recombination of $C_2H_4I_2^*$, which loses energy to the solvent through collisions in a few picoseconds (vibrational cooling). Consequent-

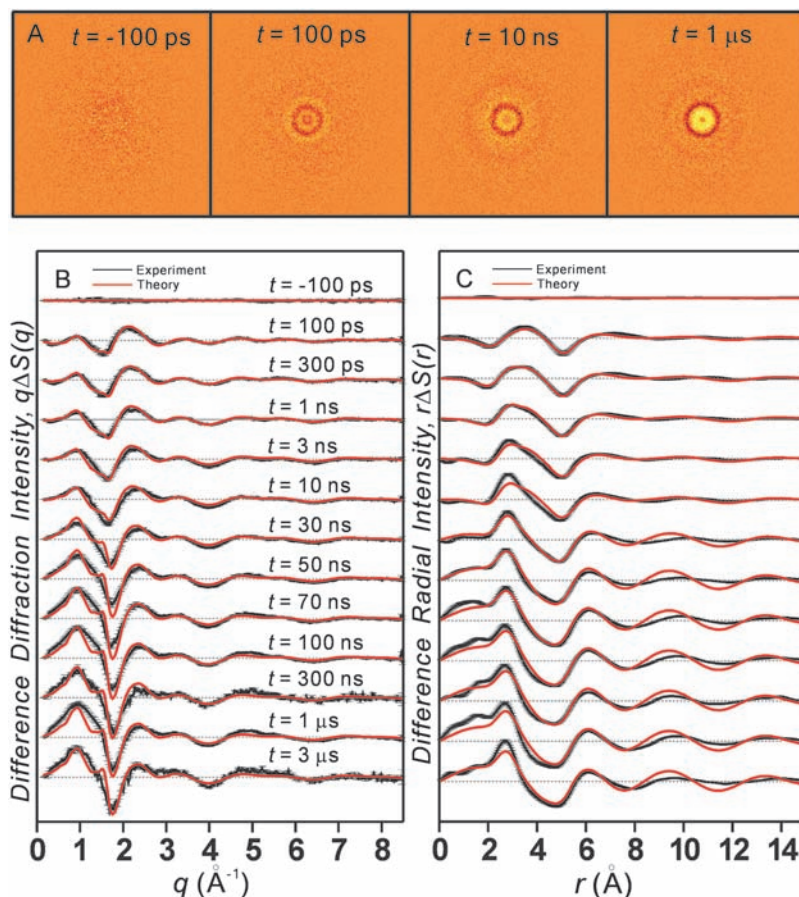


Fig. 1. Time-resolved diffraction signal as a function of time delay for $C_2H_4I_2$ in methanol. (A) Raw difference images for selected time delays (time $t = -100$ ps, 100 ps, 10 ns, and 1 μs). (B) Difference diffraction intensities, $q\Delta S(q)$, excited minus nonexcited. These are radial averages of the 2D images from (A). Least-square fits to a theoretical model are also shown. Error bars represent the experimental error associated with each scattering angle. (C) Difference radial density functions, $r\Delta S(r)$. These are sine-Fourier transforms of the difference intensities in (B). Error bars are also given to indicate the error in the real space representation.

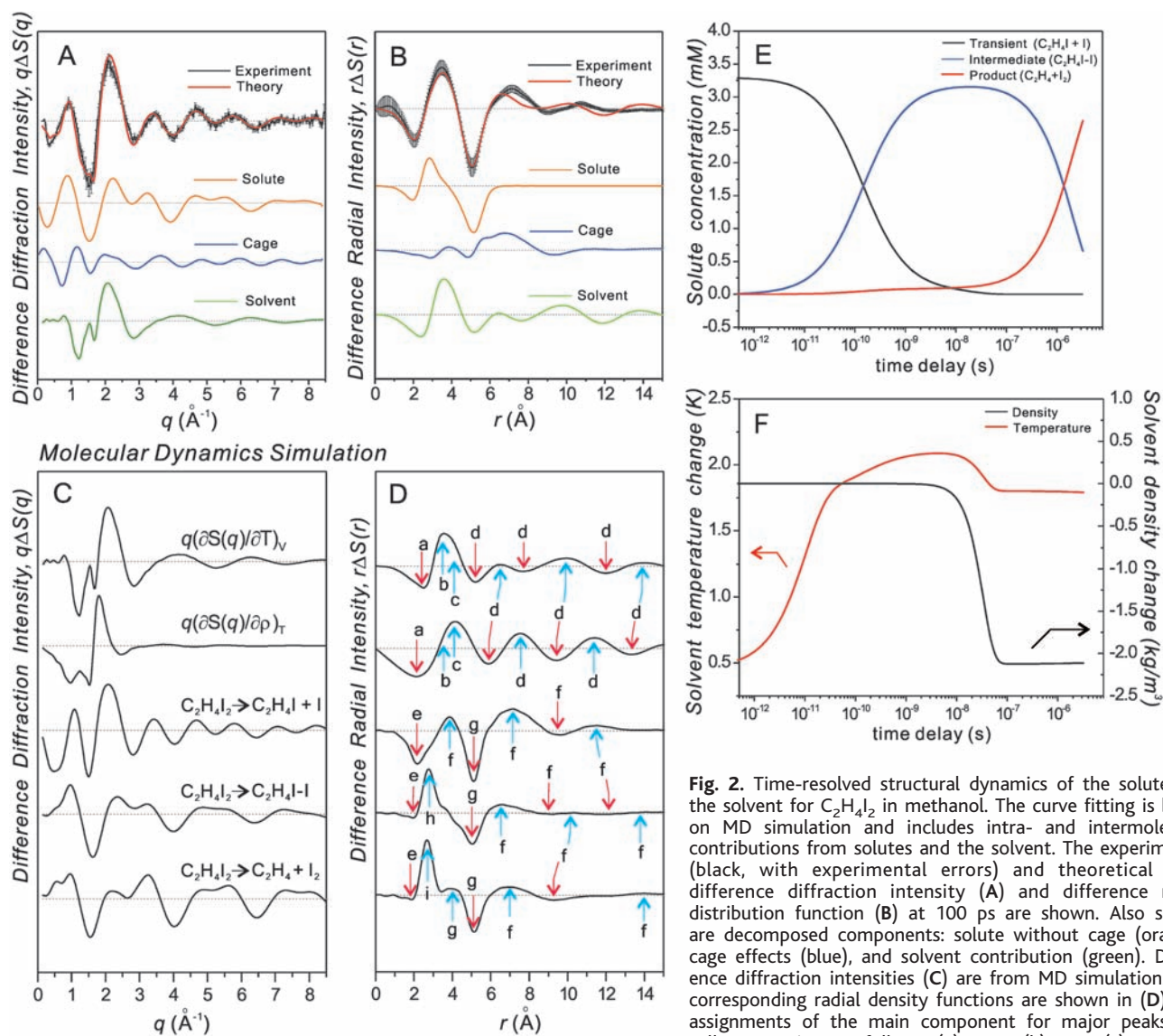
ly, 60% of the initially excited $C_2H_4I_2^*$ molecules decay directly to the ground state [see (27) for details on the analysis of this contribution].

After the major thermal expansion has started, the change in bulk density dominates the signal. However, at early times, the structural change in the bulk is relatively smaller than at later times, and the solute and cage dynamics dominate because of the heavy iodine atoms in the solute. The data can therefore be decomposed into the change in the solute only, the change in the solvation cage, and the solvent response (Fig. 2, A and B). This decomposition helps the assignment of the peaks and valleys in Fig. 2B. The negative peak around 5 Å is mainly due to the change in the solute only, and the positive peak around 7 Å is mainly due to the change in the solvation cage. The

positive peak near 4 Å is due to the change in the solvent. One cage splits into two smaller cages, with the overall effect of increasing the solute/solvent coordination number and shifting the distance distribution between the solute and solvent. As a consequence, the relative population of $I \cdots O_{\text{solvent}}$ and $I \cdots C_{\text{solvent}}$ distances increases around 4, 7, and 11 Å and decreases around 9 and 13 Å (Fig. 2B). The data offer a direct visualization of the change in the solvent cage; i.e., the change in solvent packing around the excited solutes.

In view of the complex interplay of factors contributing to these data, we could not refine molecular structures comparably to a single-crystal study. Instead, we compared our data to the calculated (ab initio and density functional theory) lowest-energy bridged and anti geom-

etries. Figure 3 shows the ratio of the statistical significance, χ^2 , for the fit using the bridged model and that using the anti model for all investigated time delays. As the concentration of $C_2H_4I_2$ decreases, the ratio expectedly approaches 1. However, below 1 ns, where $C_2H_4I_2$ is the major component, the ratio is significantly less than 1. To be sure that the experimental setup did not bias the result, we collected, in a separate experiment with a modified setup, the time delays ranging from -100 ps to 1 ns in steps of 25 ps, and the results are shown in the inset of Fig. 3. All time points below 1 ns have the ratio well below 1, thus confirming that the bridged structure reproduces the experimental curves with higher fidelity than does the anti structure. The apparent falling edge between -50 and 50 ps is due to the temporal profile of the x-ray pulse.



$O \cdots O$ and $O \cdots C$, (e) $C \cdots I$ of $C_2H_4I_2$, (f) $I \cdots O_{\text{solvent}}$ and $I \cdots C_{\text{solvent}}$, (g) $I \cdots I$ of $C_2H_4I_2$, (h) $I \cdots I$ of C_2H_4I-I , and (i) $I \cdots I$ of I_2 . (E) The population change of the transient C_2H_4I (black), the intermediate isomer C_2H_4I-I (blue), and the final product, I_2 (red), as a function of time delay. (F) The change in the solvent density (black) and the solvent temperature (red). This time behavior is well described by an exponential function with a time constant of 33 ± 5 ns, which is typical of thermal expansion. Arrows point to the corresponding axis of each curve.

If we include a mixture of the anti and bridged forms in the fit, the fraction of the anti form converges to zero.

The distinction between fits to the bridged and anti forms is emphasized when the contribution of C_2H_4I alone is carefully extracted, by subtracting from the original data other contributions of solvent, cage, and other nascent solutes, and the high q range is used to deduce the transient-only structural changes. This approach allows the transient C_2H_4I to be modeled as a naked gas-phase structure (11).

Fig. 3. The bridged model versus the anti model. The data were fit to both models and the final figures of merit (χ^2) were compared as a ratio. Below 1 ns, where the concentration of C_2H_4I is high, the ratio is significantly below 1, confirming that the bridged model fits the data better than the anti model. The inset shows the results from a separate experiment including more time points below 1 ns, which supports the above conclusion.

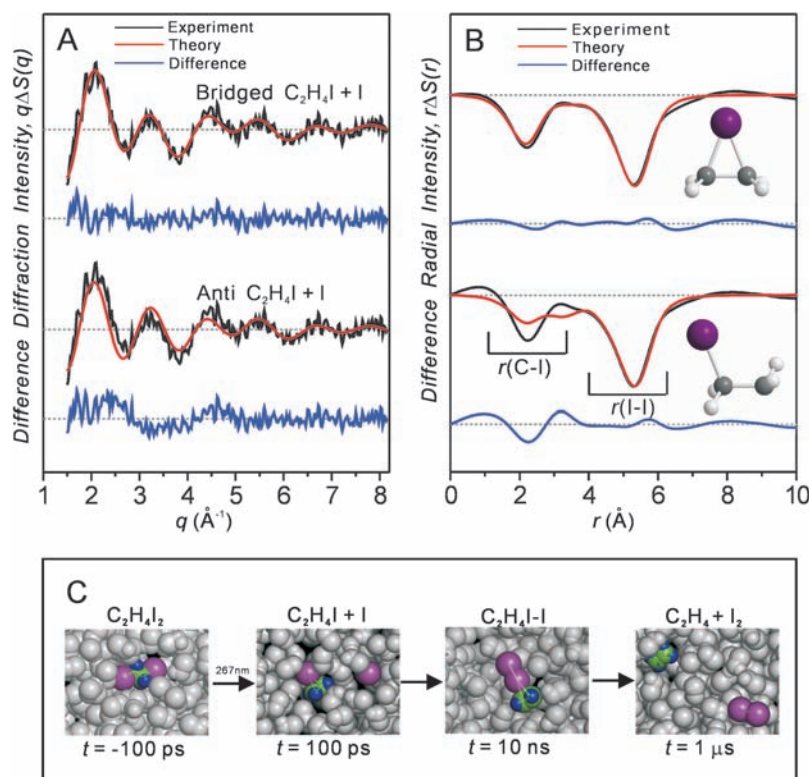
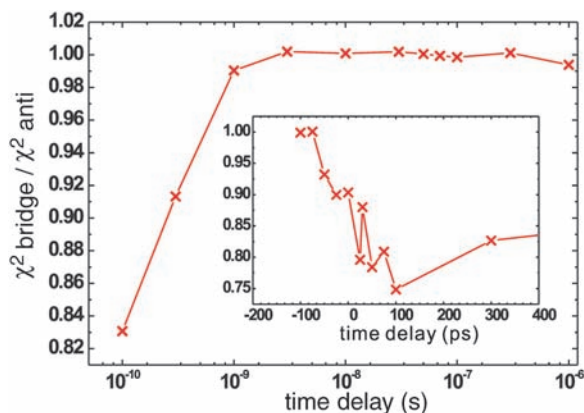


Fig. 4. (A and B) Structure determination of the C_2H_4I radical in methanol at $t = 100$ ps. The contribution from C_2H_4I alone is isolated by subtracting other contributions from the raw data, allowing comparison with the gas-phase model of the anti and bridged structures. (A) Theoretical (red) and experimental (black) difference intensities for two possible reaction channels. The differences between the theory and experiment are also shown in blue. The upper curves are for the formation of the bridged C_2H_4I radical and the lower ones are for the classical anti structure. (B) Corresponding radial density functions for the two possible reaction channels, and molecular structures (iodine, purple; carbon, gray). (C) A schematic reaction mechanism based on time-resolved x-ray diffraction in solution.

For the data at 100 ps, the experimental and theoretical curves for the putative reaction channels (Fig. 4) visually demonstrate the validity of the bridged structure against the classical anti structure. The negative peak near 5 Å corresponds to the depletion of the I...I internuclear distance in the parent molecule. This feature is common for all reaction channels, and both models agree with the data in this region. The peaks between 1 and 3 Å—the fingerprint region—are sensitive to the position of the I atom relative to the two

carbon centers. The bridged structure gives only a single peak in the fingerprint region, and our data reproduce the feature with high accuracy, whereas the anti structure gives two overlapping peaks, which is in stark contrast to the experiment. We consider the formation of $C_2H_4I^+$ ions, rather than neutral radicals, unlikely, because the C-I distance for the ion (~ 2.25 Å) is much smaller than that determined for the radical (~ 3.06 Å) from our data (30).

References and Notes

- P. Allen, D. J. Tildesley, *Computer Simulation of Liquids* (Clarendon Press, Oxford, 1989).
- C.-Y. Ruan, V. A. Lobastov, F. Vigliotti, S. Chen, A. H. Zewail, *Science* **304**, 80 (2004).
- B. J. Sivick, J. R. Dwyer, R. E. Jordan, R. J. D. Miller, *Science* **302**, 1382 (2003).
- H. Ihee *et al.*, *Science* **291**, 458 (2001).
- R. C. Dudek, P. M. Weber, *J. Phys. Chem. A* **105**, 4167 (2001).
- C. Rischel *et al.*, *Nature* **390**, 490 (1997).
- F. Schotte *et al.*, *Science* **300**, 1944 (2003).
- I. V. Tomov, D. A. Qulianov, P. Chen, P. M. Rentzepis, *J. Phys. Chem. B* **103**, 7081 (1999).
- C. Rose-Petruck *et al.*, *Nature* **398**, 310 (1999).
- C. W. Siders *et al.*, *Science* **286**, 1340 (1999).
- A. Plech *et al.*, *Phys. Rev. Lett.* **92**, 125505 (2004).
- S. Gnanakaran, R. M. Hochstrasser, *J. Am. Chem. Soc.* **123**, 12886 (2001).
- A. B. Vakhtin, J. E. Murphy, S. R. Leone, *J. Phys. Chem. A* **107**, 10055 (2003).
- M. Rasmuson, A. N. Tarnovsky, T. Pascher, V. Sundstrom, E. Akesson, *J. Phys. Chem. A* **106**, 7090 (2002).
- J. K. Kochi, Ed., *Free Radicals* (Wiley, New York, 1973), vol. II.
- A. L. J. Beckwith, K. U. Ingold, in *Rearrangements in Ground and Excited States*, P. d. Mayo, Ed. (Academic Press, New York, 1980), vol. 1, pp. 273–275.
- J. Fossey, D. Lefort, J. Sorba, Eds., *Free Radicals in Organic Chemistry* (Wiley, New York, 1995).
- H. L. Goering, P. I. Abell, B. F. Aycock, *J. Am. Chem. Soc.* **74**, 3588 (1952).
- W. Thaler, *J. Am. Chem. Soc.* **85**, 2607 (1963).
- P. S. Skell, D. L. Tuleen, P. D. Readio, *J. Am. Chem. Soc.* **85**, 2849 (1963).
- B. Engels, S. D. Peyerimhoff, *J. Mol. Struct.* **138**, 59 (1986).
- F. Bernardi, J. Fossey, *J. Mol. Struct.* **180**, 79 (1988).
- H. Ihee, A. H. Zewail, W. A. Goddard III, *J. Phys. Chem. A* **103**, 6638 (1999).
- A. J. Bowles, A. Hudson, R. A. Jackson, *Chem. Phys. Lett.* **5**, 552 (1970).
- D. J. Edge, J. K. Kochi, *J. Am. Chem. Soc.* **94**, 6485 (1972).
- S. Paul Maj, M. C. R. Symons, P. M. R. Trousson, *Chem. Commun.* 561 (1984).
- Materials and methods are available as supporting material on Science Online.
- S. Bratos, F. Mirloup, R. Vuilleumier, M. Wulff, A. Plech, *Chem. Phys.* **304**, 245 (2004).
- S. Aditya, J. E. Willard, *J. Am. Chem. Soc.* **79**, 2680 (1957).
- The least-squares fit gives a C-I bond length of 3.06 ± 0.02 Å in the bridged structure, as compared with a theoretical value of 3.11 Å. The CCI angle is $77.2 \pm 0.1^\circ$. The errors are 1 SD in the fit, and they do not account for systematic errors. The C-I bond distance in the parent molecule, 2.17 ± 0.01 Å, is also slightly smaller than the theoretical value of 2.20 Å. The complete dissociation to $C_2H_4 + 2I$ does not fit our experimental data. Moreover, the inclusion of a gauche component in the population of the parent molecules ($C_2H_4I_2$) makes the fit worse, indicating that the majority of the parent molecules adopt the anti rather than the gauche form, in agreement with the calculated energy difference of 13 kJ/mol.
- We thank R. Vuilleumier and F. Mirloup for invaluable help in developing the theoretical

framework for time-resolved x-ray diffraction from liquids, including MD simulations, and P. Anfinrud, F. Schotte, A. Plech, and A. Cupane for discussions and assistance. This work was supported by the Korea Research Foundation Grant funded by Korean Government (Ministry of Education and Human Resources Development) grant no. R08-2004-000-10076-0 to H.I. and by the European Union grant nos. HPRI-CT-

1999-50004 and HPRN-CT-00160. H.I. also acknowledges support from the Korea Advanced Institute of Science and Technology (KAIST) and from fellow faculty members in the KAIST chemistry department.

Supporting Online Material
www.sciencemag.org/cgi/content/full/1114782/DC1

Materials and Methods
Figs. S1 to S11
References and Notes

12 May 2005; accepted 30 June 2005
Published online 14 July 2005;
10.1126/science.1114782
Include this information when citing this paper.

Theoretical Study of Geometric Phase Effects in the Hydrogen-Exchange Reaction

Juan Carlos Juanes-Marcos,¹ Stuart C. Althorpe,^{1*} Eckart Wrede²

The crossing of two electronic potential surfaces (a conical intersection) should result in geometric phase effects even for molecular processes confined to the lower surface. However, recent quantum simulations of the hydrogen exchange reaction ($\text{H} + \text{H}_2 \rightarrow \text{H}_2 + \text{H}$) have predicted a cancellation in such effects when product distributions are integrated over all scattering angles. We used a simple topological argument to extract reaction paths with different senses from a nuclear wave function that encircles a conical intersection. In the hydrogen-exchange reaction, these senses correspond to paths that cross one or two transition states. These two sets of paths scatter their products into different regions of space, which causes the cancellation in geometric phase effects. The analysis should generalize to other direct reactions.

Recent work (1) has established that conical intersections (CIs) play a central role in the dynamics of many chemical reactions and photoprocesses. At a CI, two electronic states touch, so that the Born-Oppenheimer approximation (that electronic and nuclear motion are separable) breaks down. A system with a CI can therefore convert rapidly between elec-

tronic states by passing through the intersection. Such rapid switching is exploited in many light-harvesting and charge-transfer processes. Another consequence of the Born-Oppenheimer breakdown is the geometric (2–6) [or Berry (7)] phase (GP), which occurs even if the system is confined to the lower electronic surface and avoids the neighborhood

of the conical intersection. The GP is the sign change (or π phase shift) acquired by the electronic wave function Φ , when the nuclei complete an odd number of loops around the CI. The GP produces a corresponding sign change in the boundary condition of the nuclear wave function Ψ (4–6), in order to make the total wave function ($\Phi\Psi$) single-valued (i.e., uniquely specified at each nuclear geometry). As a result, even without electronic excitation, the vibrational and rotational motions on the lower electronic state are changed by the proximity of a CI. The implications of such changes for chemical reactivity are poorly understood.

In isolated molecules, the effects of the GP are reasonably well understood, thanks mainly to detailed experiments and theoretical predictions on Jahn-Teller systems (6, 8). In the simplest “particle on a ring” system, the effect of the GP is to switch the allowed quantum numbers of the nuclear wave function from integer to half-integer values. Comparable shifts

¹School of Chemistry, University of Nottingham, University Park, Nottingham, NG7 2RD, UK. ²Department of Chemistry, University of Durham, South Road, Durham, DH1 3LE, UK.

*To whom correspondence should be addressed. E-mail: stuart.althorpe@gmail.com

